Volume compensation of large-deformation 3D-printed soft elastomeric elastocaloric regenerators

Kun Wang,[1] Johannes T.B. Overvelde,[2] Kurt Engelbrecht,[1] Rasmus Bjørk,[1] and Christian R.H. Bahl[1]
[1)]*Department of Energy Conversion and Storage, Technical University of Denmark, Anker Engelunds Vej 301, 2800 Kgs. Lyngby, Denmark*
[2)]*Autonomous Matter Department, AMOLF, 1098XG Amsterdam, The Netherlands*

(*Electronic mail: kunwa@dtu.dk)

(Dated: 2 November 2023)

Elastomeric elastocaloric regenerators have great potential for use in low-stress elastocaloric cooling devices. However, these regenerators display an asymmetric fluid exchange when operating in an active elastocaloric cooling cycle, due to the large required strains and associated volume change. During strain, the fluid volume increases, which passively forces fluid flow into the regenerator; when the strain is released, the fluid volume decreases, which results in a fluid flow out of the regenerator. During a traditional elastocaloric cooling cycle, there are also active fluid flow periods provided by fluid displacers or pumps. Here we study the passive fluid flow in high-strain regenerators using a numerical model and experiments in two types of regenerators. Hyperelastic models are used to fit the experimentally measured mechanical behavior of thermoplastic polyurethane elastocaloric elastomers, and the model is subsequently used to conduct finite-element simulations predicting regenerator volume changes for an applied strain of 200-600%. We validated the results using a specifically designed setup for measuring volume changes using pressure differences on a parallel-plate regenerator. For a strain range of 200-600%, the predicted volume change ratio is 69.5%, closely matching the experimental value of 66.7%. We observed that the middle region of the regenerator experiences a higher volume change, which can be accurately accounted by the numerical model.

Elastocaloric materials (eCMs) that exhibit temperature increase and decrease in response to a unaxial strain loading/unloading have seen a growing interest in recent years, especially as a promising alternative to conventional vapor-compression refrigerants. As elastocaloric cooling cycles are based on a solid-state refrigerant in contact with a water-based heat transfer fluid, the technology will have a lower global warming potential than refrigerants used in vapor compression[1–3]. Elastocaloric cooling is considered one of the promising solid-state refrigeration technologies (i.e. magnetocaloric[4–6], electrocaloric[7,8], elastocaloric[9–12], and barocaloric[13,14]) and can potentially have a higher coefficient of performance (COP) and a net-zero greenhouse gas emission[15,16]. Elastocaloric cooling specifically was selected as the most promising non-vapor compression refrigeration technology by the US Department of Energy in 2014[17]. The investigation of high-performance elastocaloric materials and regenerators is crucial for driving the progress and widespread adoption of elastocaloric cooling technologies.

Soft elastomers, such as natural rubbers, thermoplastic polyurethane (TPU), and synthetic polymers, have recently emerged as potential materials for elastocaloric applications in cooling and heating[18–22]. These materials exhibit much lower applied stress requirements to trigger the elastocaloric effect (eCE), typically several MPa or even less. In contrast, elastocaloric alloys require several hundred MPa of applied stress, highlighting the need for mechanically robust systems[10,16,23]. Overcoming the challenge of high applied stress remains an ongoing engineering endeavor in elastocaloric refrigeration, hindering the miniaturization of cooling systems and limiting their potential applications. Recently, elastocaloric cooling prototypes using soft elastomers have been demonstrated with a comparably high COP = 6 and temperature span >8 K[20,21,24], which provides an avenue for developing lower-stress and miniaturized eCE devices.

Active caloric regenerators act as a combination of refrigerant and heat exchangers, and can extend the operating temperature span for the thermodynamic cycle[25,26]. The heat generation and absorption as well as exchange between the source and sink take place in the regenerator structure. Over the past few decades, significant research efforts have been dedicated to exploring and constructing improved heat-transfer mechanisms and robust mechanical structures for magnetic and elastocaloric regenerators[27–30]. In recent years, additive manufactured (AM) technologies have become mature and especially adept at fabricating complex 3D structures, capable of increasing freedom of the structural design. There are an increasing number of studies with the goal of implementing AM methods to the fabrication of caloric regenerators or caloric materials preparation, some of which shows satisfactory or even enhanced performance compared to traditional regenerators[22,29,31]. Our previous studies show the great potential to implement AM to fabricate full-scale active eCE regenerators, potentially improving the temperature span[22].

Operating as an active eCE regenerator, elastomer-based regenerators are subjected to four steps: loading, the cold-to-hot blow (cold blow), unloading, and hot-to-cold blow (hot blow). Figure 1 **a** illustrates the fluid-channel volume change evolution over an elastocaloric thermodynamic cycle. The temperature variation associated with corresponding loading-unloading steps of elastocaloric elastomers is shown in Figure 1 **b** as obtained from our previous work[22]. During the first process 1 to 2, the regenerator is stretched resulting in a temperature increase. At the same time the fluid-channel volume increases as the regenerator undergoes large strains, as shown in Figure 1 **a**. The volume change is expressed as $V_f - V_i$ indicating the difference of the final and initial fluid-channel volume.

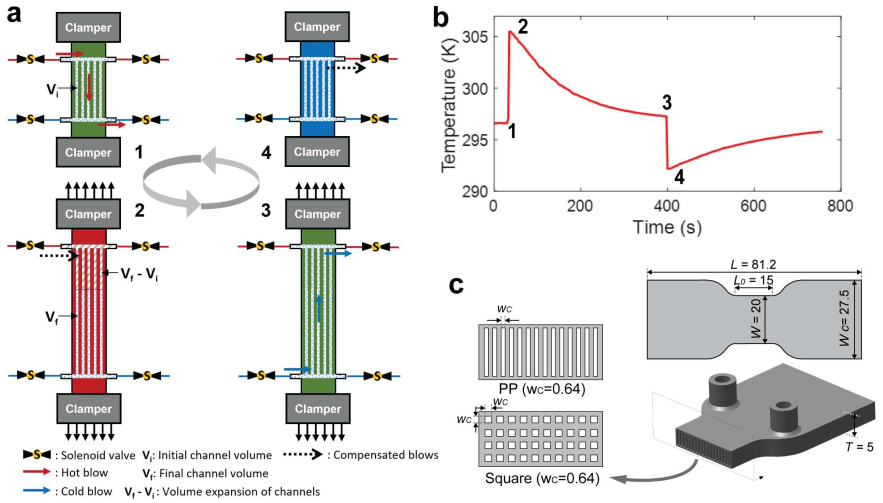

FIG. 1. Schematic illustration of the volume change induced by large deformation and the corresponding steps in an elastocaloric cycle, **a** and **b**; schematic regenerator and two selected fluid channels labeled with the related geometric dimension (unit in mm), **c**. Note that the schematic channels differ from the real numbers of channels, which are 18 for PP channels and 18×5 for square channels.

Importantly, it can been observed in a rubber-tube eCE cooler and in elastomers[24,32] that large strains cause the volume of fluid channels to change in an unclear manner which results in asymmetric hot and cold blows as well as potentially unwanted heat transfer between the fluid and eCM during the loading and unloading processes. However, this effect has never been specifically investigated.

In this work, we study the volume change produced by the large deformation in elastomeric regenerators both experimentally and numerically to understand how to realize a regenerative elastocaloric cooling system with continuous fluid compensations. We study different fluid channels to investigate the geometrical impacts on volume changes, as illustrated in Fig. 1. Hyperelastic models are implemented in finite element (FE) simulations to predict volume changes of eCE regenerators. The corresponding regenerators are 3D-printed for validation of volume changes under large deformations.

The extra increased volume should be compensated to ensure the best-possible fluid flow profile throughout the cycle. In continuous flow systems, compensating for volume increases of the channel is typically inevitable due to the resulting negative pressure. Accordingly, a tailored fluidic compensation strategy can be devised to accommodate this volume change. The strategy involves managing compensations from the hot or cold reservoirs during the loading process and returning them to the reservoirs during the unloading process, depending on the specific cooling or heating implementations. Quantifying the amount of compensation volume is necessary for the development of high-performance regenerative elastomeric eCE regenerators.

We consider two typical regenerator fluid channels, namely parallel-plates (PP) and square channels, as shown in Figure 1 **c**. For both regenerator geometries, the external regenerator shape is a dogbone to avoid stress concentrations. The PP regenerator comprises 18 identical channels with a height of 4 mm while the square channel regenerator consists of 18×5 channels uniformly distributed in the regenerator. Both the PP channel and the square channel have a channel length of 36 mm in the same regenerator shape.

TPU possesses various complex mechanical properties such as hysteresis, softening, Mullins effect, time dependence[33,34]. In this study, we have simplified the constitutive model based on the actual operating conditions of eCE regenerators. These regenerators undergo alternating loading and unloading at a constant strain rate, ultimately reaching a steady thermal exchange status and mechanical equilibrium. To accurately capture the fluid-channel volume change during cyclic loading, we start with FE simulations by employing hyperelastic constitutive models to fit the equilibrium stress-strain response for large-deformation eCE regenerators. Explicit FE methods are implemented in the simulation for the volume change predication. Hyperelasticity is also commonly employed to simplify phenomenological models for rubber-like materials[35–37].

We use hyperelastic constitutive models to fit the uniaxial stress-strain response of the elastocaloric TPUs. The hyperelastic model is based on different strain potential density functions, W. We assume that our printed elastomers are isotropic. The constitutive relationship based on the theory of continuum mechanics can then be expressed by the three invariants of the right Cauchy-Green deformation tensor $\mathbf{C}$[38]. For

rubber-like elastomers during uniaxial tensile tests, the mechanical response is close to incompressibility (J = 1) under small stretches. However, when applying large strains, Poisson's ratio and mechanical responses will be highly strain-dependent[39,40]. For our cases, the applied strain reaches large strains 500-600% where volume changes play an important role and the incompressibility constraint is no longer satisfactory. Here we choose the Mooney-Rivlin model and Ogden model to fit the stress-strain response of TPU elastomers. The Mooney-Rivlin strain energy function can be expressed as[41]:

$$W = \sum_{i,j=0}^{N} C_{ij} (\bar{I}_1 - 3)^i (\bar{I}_2 - 3)^j + \sum_{i=1}^{N} \frac{1}{d_i} (J-1)^{2i}, \quad (1)$$

and the Ogden strain energy function can be expressed as[42]:

$$W = \sum_{i=1}^{N} \frac{\mu_i}{\alpha_i^2} \left(\bar{\lambda}_1^{\alpha_i} + \bar{\lambda}_2^{\alpha_i} + \bar{\lambda}_3^{\alpha_i} - 3 \right) + \sum_{i=1}^{N} \frac{1}{d_i} (J-1)^{2i}. \quad (2)$$

In these strain energy function expressions, the invariants are modified in principal stretches (marked with the overline) form based on the deviatoric-volumetric multiplicative split for compressible material models[39,43]. See details in methods of supplementary information.

To approach stabilized mechanical behavior, the standard sample was loaded for 20 cycles at a strain rate of 1 s^{-1} which reaches equilibrium, as shown in Figure 2 **a** (see experimental details in the supplementary information). The performed strain range 0-500% is based on our desired operating range for a prototype. The equilibrium stress-strain response of loading process of the 20th cycle is employed for the hyperelastic model fitting by removing the creep regime. Basically, this bucking is always observed due to creep caused extension, even upon full contraction of the loading conditions. The fitting results are shown in Fig. 2 **b**. The fitting error can be evaluated as:

$$\text{error } (\%) = \frac{\int_{\varepsilon_0}^{\varepsilon} |\sigma_{\text{sim}} - \sigma_{\text{exp}}| \, d\varepsilon}{\int_{\varepsilon_0}^{\varepsilon} \sigma_{\text{exp}} d\varepsilon} \times 100\% \quad (3)$$

The fitting parameters for these four models are summarized in the table I. Comparing the fitting results, the N=5 Ogden model achieves the best fitting and is therefore implemented in the FE simulation for the 3D-printed regenerator fluid-channel volume change prediction.

Next, a FE modeling of the regenerator to find the volume change was conducted. Half of the regenerator was modelled due to the symmetry and the inlet structures were also neglected in the simulation. We applied a strain in a sequence from 0 to 600% and the volume change ratio ($\delta V = \frac{V_f - V_i}{V_i} \times 100\%$) calculated is shown in Figure 3 **a** and **c**. It can be seen that the volume change ratio in the PP-channel regenerator is higher than that of the square channel. Furthermore, the PP channel has a higher stress in the middle active region of the regenerator due to its smaller cross-sectional area.

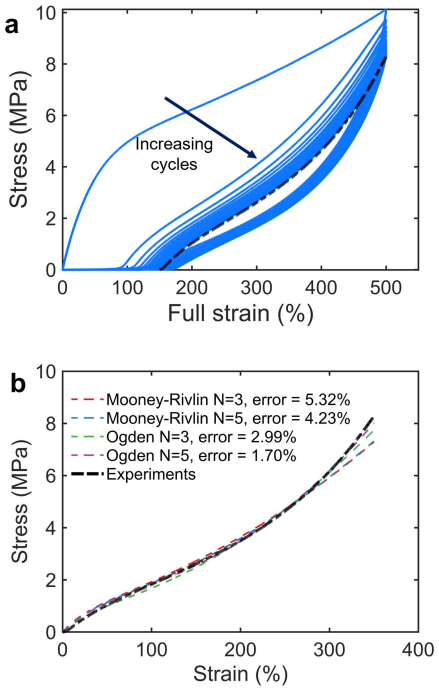

FIG. 2. Hyperelastic model fitting for the stress-strain response of TPU elastomers: **a** 20 tensile cycles (blue) with the equilibrium curve for fitting (black); **b** Comparison of hyperelastic fittings.

In principle, the stress should be similar. But this section is softer due to less material, thus more deformation goes there, so it should experience a higher stress. To visualize the fluid channels geometry variation under large deformation, the fluid channels of the initial and final states at a strain of 600% are shown in Figure 3 **b** and **d** for PP channels and square channels, respectively. Comparing the deformed channels in Figure 3 **a** and **b**, we observe that the PP channels are subject to a buckling along the Z-axis (thickness direction) which is significant at the boundary channels while this is not observed for the square channels. This buckling might be the reason of the observed reduction in stability in the Z-axis of thin plate walls between the channels when undergoing a large uniaxial strain[44]. As a consequence, the PP channel buckling contributes to an increased volume change ratio in the PP channels. In addition, higher strains (∼53 mm, 600%) are obtained by PP channels.

To validate the simulation results, experimental measurements were conducted to determine the actual volume change

TABLE I. The fitting results list of the different hyperelastic models with different parameter numbers

Hyperelastic models	Number	List of parameters										
Mooney model	N=3	C10	C01	C11	d_1							
		0.205	0.458	0.051	5.385e-05							
	N=5	C10	C01	C20	C11	C02	d_1					
		0.414	0.228	0.041	0.048	5.994e-4	0.159					
Ogden model	N=3	μ_1	α_1	μ_2	α_2	μ_3	α_3	d_1				
		50.515	0.048	0.048	4.796	-0.052	-0.382	0.167				
	N=5	μ_1	α_1	μ_2	α_2	μ_3	α_3	μ_4	α_4	μ_5	α_5	d_1
		1.556	0.397	0.397	2.835	0.005	7.489	2.835	0.326	2.285	0.035	1.003

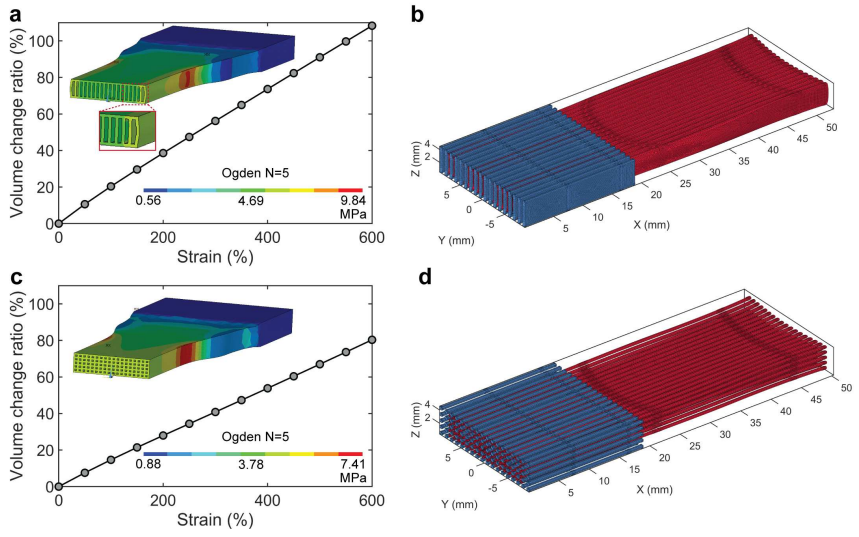

FIG. 3. Simulation results for PP channels **a** and square channels **c** volume change prediction as a function of strain (Von Mises stress at 600% for the insets), and corresponding 3D-fluid channels **b** and **d** under 600% strain where X = 0 mm is symmetric plane (Y-Z) and the clamped area is at X = 25.5 mm and X = 85.5 mm for initial (blue) and deformed (red) channels (there is a 7.5 mm distance between the channel end and clamped area before loading).

of the fluid channels during the stabilized mechanical process. The experimental setup was designed based on pressure difference measurements (see details in supplementary information). The idea is to apply the same pressure to the regenerator and the air tank 2 (reference pressure) when the pressure gets stabilized to seal the regenerator as a closed volume. During the loading process, the volume change can be determined by monitoring pressure changes between the regenerator and air tank 2. The experimental fluidic system shown in Figure 4 **a** and Figure 4 **b** is the physical setup, where the regenerator pressure is denoted as *P1* and the reference pressure from air tank 2 is denoted as *P2*. The volume change ratio can be calculated based on the ideal gas law equation ($PV = nRT$):

$$\delta V = \frac{V_f - V_i}{V_i} = \frac{P_i}{P_f} - 1 = \frac{P_2}{P_1} - 1. \tag{4}$$

Taking into account impacts from the temperature changes of the regenerator and the connected tubes volume between the regenerator and the pressure sensor, the actual volume change ratio of the regenerator can be calibrated to be (see details in supplementary information about pressure change calibrations):

$$\delta V_R = (1 + \frac{1}{\alpha})(C\frac{P_i}{P_f} - 1), \tag{5}$$

in which α and C are the temperature and volume calibration ratio, respectively. The temperature ratio (C) is defined as:

$$C = \frac{P_f V_f}{P_i V_i} = \frac{T_f}{T_i}. \tag{6}$$

The volume ratio between regenerator channels and connec-

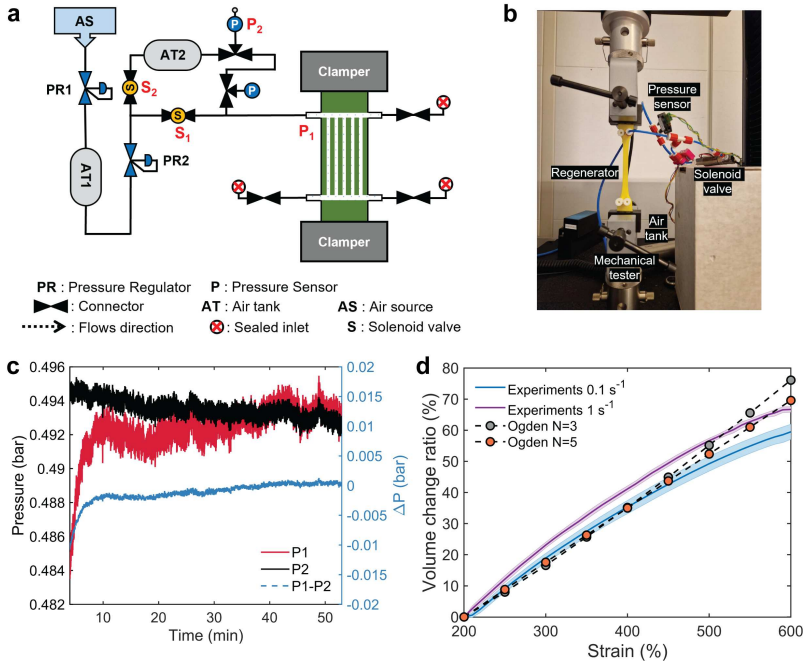

FIG. 4. Pneumatic experimental setup and simulation validation: **a**. Fluidic circuit for pressure difference measurements (P1: regenerator pressure, P2: air tank 2 pressure); **b**. Physical picture for the setup; **c**. Airtight examination by monitoring pressure holding; **d**. Comparison of volume change ratio as a function of strains at different loading rates (simulations performed at 1 s^{-1} loading rate).

tion tubes is define as α,

$$\alpha = \frac{V_R}{V_{\text{tube}}}. \tag{7}$$

The α value is 0.985 for PP channels and the C value is 1.01 at 600%.

The PP regenerator is employed for the volume-change validation experimentally. Before measurements, the airtightness of the device and the regenerator need to be ensured. We applied a 0.5 bar pressure to tank 2 and the regenerator and closed the two solenoid valves (at 20 min in Figure 4 **c**) and waited for 30 min to confirm the pressure maintenance. The results of pressure differences ($P1-P2$) is stabilized approaching to zero indicating no air leakage in the regenerator and thus a good airtightness of the sample. The volume change measurements are performed under cyclic operation along X-axis at different strain rates for a strain range of 200-600% to avoid creep. The volume change ratio as a function of strain at rates of 0.1 s^{-1} and 1 s^{-1} is shown in Figure 4 **d** along with the simulation results normalized to 200% strain to remove the creep regime. From the experimental results at different loading rates, the higher loading rate shows a larger volume change ratio. From the experimental results, we noticed that the regenerator subjected to a higher loading rate exhibited a larger volume change ratio. This is because the lower loading rate allows more creep deformation to occur[33,45]. The simulation results at 1 s^{-1} were slightly lower than the experimental results overall. This difference could be because the simulations did not include certain connecting structures between the regenerator fluid channels and the fluid inlet and outlet, which were present in the experiments, and could also be that in experiments the cross-section is different due to the printing. Here the Ogden model was applied to the simulation for comparison. It is noteworthy that the Ogden 3 and 5 models provide satisfactory predictions for the regenerator volume change in our desired operating range. When strains exceed 500%, there is an over estimation for Ogden 3 due to the constrained strain range (500%) employed for the hyperelastic fittings in Figure 2. It can be anticipated that by employing a larger strain range during the hyperelastic model fitting, more accurate predictions can be obtained.

Operating in an eCE cycle, the ratio (V^*) of displaced fluid volume (V_{disp}) and regenerator volume (V_R) or Utilization are one of evaluating factors for the eCE regenerator performance to measure how much heat extracted from the regenerator by heat-transfer fluids[12,46,47]. The V^* shows to be 1 for the best COP in a NiTi-based prototype at 1.7 %[46], which means the same V_{disp} and V_R. In this volume increased case, the V^* can

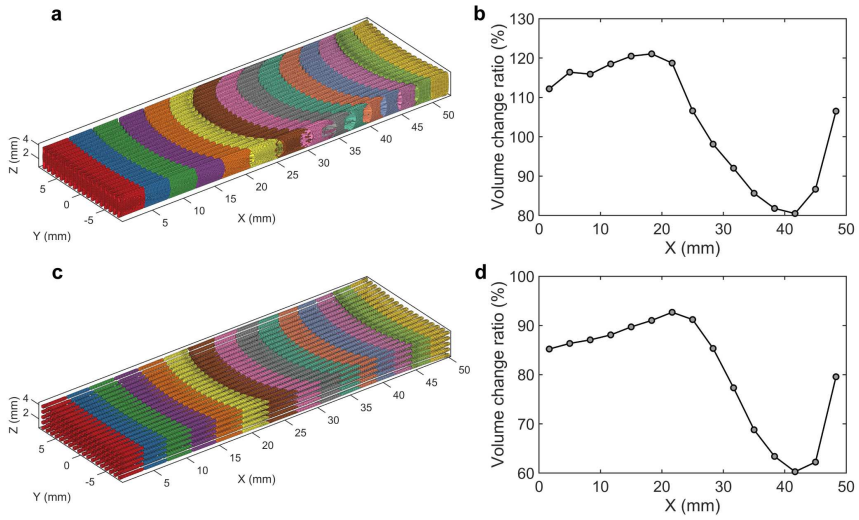

FIG. 5. Volume change distribution (volume change as a function of the X coordinate at 600%) along the tensile direction for the different volume channels: **a** and **b** for the parallel-plate channel; **c** and **d** for the square channel; in the figure of 3D-fluid channels Y-Z is symmetric plane and X = 85.5 mm is clamped area (actually, there is a 7.5 mm distance between the channel end and clamped area).

be rewritten as:

$$V^* = \frac{V_{disp}}{0.5 \times (V_{R,i} + V_{R,f})} = \frac{V_{disp}}{V_{R,i} + 0.5 V_{R,i} \delta V_R}. \quad (8)$$

For the PP regenerator, with a δV_R of 66.7% the equivalent V^* will be 0.74, indicating decrease in V^* when the fluidic channel volume increases by large deformation. In previous regenerative coolers[12,24], it has been demonstrated that the optimized V^*/Utilization ratio provides enhanced cooling power and temperature span. However, this strain-induced volume change leads to the deviatoric V^* and asymmetric hot-cold blows and further will reduce the temperature span. It suggests a tailored flow system allowing compensating this volume change to maintain a satisfactory temperature span during practical operation.

In an actual 3D printed elastocaloric regenerator, the volume change also may be position-dependent. Simulation results can quantify the volume change distribution along the tensile direction. We consider the fluid channels segmented into 15 segments to examine the volume change distribution along the tensile axis. Figure 5 **a** and **c** show the results for the PP channels and square channels under 600% strain and the volume change ratio of each segment is plotted in Figure 5 **b** and **d**. We observed after 20 mm of regenerator length the volume change ratio gradually decreases in a certain coordinate range for both PP channels (up to 48 mm) and square channels (up to 40 mm) and then slightly increases. This decrease in volume change along the regenerator length direction is due to the compression exerted by the rounded section of the dogbone-shaped regenerator, by observing deformed structures in Figure 3 **a** and **c**. The volume change ratio increases at the channel end could be attributed to the boundary effect near the clamped side.

In conclusion, Ogden hyperelastic models achieve a good fit for the stress-strain response of eCE TPU elastomers and corresponding FE simulations for the prediction of regenerator volume compensations exhibit excellent agreement with experimental results. The PP regenerator shows higher volume change compared to the square-channel regenerator under significant deformation, due to thin-plate buckling instability. Subjecting the PP regenerator to a 200-600% strain results in a 66.7% volume change ratio. A nonuniform volume change behavior is observed along the stretching direction, particularly in the rounded region of the dogbone-shaped regenerators. These results hold promise for accurately predicting volume compensation in soft, large-deformation eCE regenerators and inspiring the design and modeling of active large-deformation regenerators.

See the supplementary information for experimental details and methods for the hyperelastic model fitting. The modeling conditions, and calibrations of pressure change measurements are also included.

K. Wang is grateful for financial support from the Otto Mønsted Foundation and China Scholarship Council scholarship. This work is part of Dutch Research Council (NWO) and was partly performed at the research institute AMOLF. We wish to acknowledge Dr. Shibo Zou for the valuable discussion on fluidic setups and Paul Ducarme and Alberto Co-

moretto for the help in FE simulations.

AUTHOR DECLARATIONS

CONFLICT OF INTEREST

The authors have no conflicts to disclose.

AUTHOR CONTRIBUTIONS

Kun Wang: Conceptualization (equal); Data curation (equal); Formal analysis (equal); Investigation(equal); Methodology (equal); Validation (equal); Software (equal); Writing – original draft(equal); Writing – review & editing (equal). **Johannes T.B. Overvelde**: Software (equal); Writing – review & editing (equal); Supervision (equal); Funding acquisition (equal). **Kurt Engelbrecht**: Writing – review & editing (equal); Supervision (equal). **Rasmus Bjørk**: Writing – review & editing (equal); Supervision (equal). **Christian R.H. Bahl**: Writing – review & editing (equal); Supervision (equal); Funding acquisition(equal).

DATA AVAILABILITY

The data that support the findings of this study are available from[48].

[1] M. O. McLinden, J. S. Brown, R. Brignoli, A. F. Kazakov, and P. A. Domanski, Nat. Commun. **8**, 14476 (2017).
[2] N. Abas, A. R. Kalair, N. Khan, A. Haider, Z. Saleem, and M. S. Saleem, Renew. Sustain. Energy Rev. **90**, 557–569 (2018).
[3] O. Secretariat, *Handbook for the montreal protocol on substances that deplete the ozone layer* (2020).
[4] V. K. Pecharsky and K. A. Gschneidner, Jr., Phys. Rev. Lett. **78**, 4494–4497 (1997).
[5] O. Tegus, E. Brück, K. Buschow, and F. De Boer, Nature **415**, 150–152 (2002).
[6] J. Liu, T. Gottschall, K. P. Skokov, J. D. Moore, and O. Gutfleisch, Nat. Mater. **11**, 620–626 (2012).
[7] B. Neese, B. Chu, S.-G. Lu, Y. Wang, E. Furman, and Q. Zhang, Science **321**, 821–823 (2008).
[8] P. Bai, Q. Zhang, H. Cui, Y. Bo, D. Zhang, W. He, Y. Chen, and R. Ma, Adv. Mater. **35**, 2209181 (2023).
[9] E. Bonnot, R. Romero, L. Mañosa, E. Vives, and A. Planes, Phys. Rev. Lett **100**, 125901 (2008).
[10] D. Cong, W. Xiong, A. Planes, Y. Ren, L. Mañosa, P. Cao, Z. Nie, X. Sun, Z. Yang, X. Hong, *et al.*, Phys. Rev. Lett **122**, 255703 (2019).
[11] S. Zhang, Q. Yang, C. Li, Y. Fu, H. Zhang, Z. Ye, X. Zhou, Q. Li, T. Wang, S. Wang, *et al.*, Nat. Commun. **13**, 9 (2022).
[12] S. Qian, D. Catalini, J. Muehlbauer, B. Liu, H. Mevada, H. Hou, Y. Hwang, R. Radermacher, and I. Takeuchi, Science **380**, 722–727 (2023).
[13] B. Li, Y. Kawakita, S. Ohira-Kawamura, T. Sugahara, H. Wang, J. Wang, Y. Chen, S. I. Kawaguchi, S. Kawaguchi, K. Ohara, *et al.*, Nature **567**, 506–510 (2019).
[14] D. Matsunami, A. Fujita, K. Takenaka, and M. Kano, Nat. Mater. **14**, 73–78 (2015).
[15] X. Moya, S. Kar-Narayan, and N. D. Mathur, Nat. Mater. **13**, 439–450 (2014).
[16] H. Hou, S. Qian, and I. Takeuchi, Nat. Rev. Mater. **7**, 633–652 (2022).
[17] U. D. of Energy, "Energy savings potential and rd&d opportunities for non-vapor-compression hvac technologies," Tech. Rep. (2014).
[18] D. Guyomar, Y. Li, G. Sebald, P.-J. Cottinet, B. Ducharne, and J.-F. Capsal, Appl. Therm. Eng. **57**, 33–38 (2013).
[19] Z. Xie, G. Sebald, and D. Guyomar, Appl. Phys. Lett. **107**, 081905 (2015).
[20] F. Greibich, R. Schwödiauer, G. Mao, D. Wirthl, M. Drack, R. Baumgartner, A. Kogler, J. Stadlbauer, S. Bauer, N. Arnold, *et al.*, Nat. Energy **6**, 260–267 (2021).
[21] S. Zhang, Q. Yang, C. Li, Y. Fu, H. Zhang, Z. Ye, X. Zhou, Q. Li, T. Wang, S. Wang, *et al.*, Nat. Commun. **13**, 9 (2022).
[22] K. Wang, K. Engelbrecht, and C. R. Bahl, Appl. Mater. Today **30**, 101711 (2023).
[23] L. Porenta, P. Kabirifar, A. Žerovnik, M. Čebron, B. Žužek, M. Dolenec, M. Brojan, and J. Tušek, Appl. Mater. Today **20**, 100712 (2020).
[24] G. Sebald, G. Lombardi, G. Coativy, J. Jay, L. Lebrun, and A. Komiya, Appl. Therm. Eng. , 120016 (2023).
[25] K. K. Nielsen, J. Tusek, K. Engelbrecht, S. Schopfer, A. Kitanovski, C. R. H. Bahl, A. Smith, N. Pryds, and A. Poredos, Int. J. Refrig. **34**, 603–616 (2011).
[26] S. Qian, J. Yu, and G. Yan, Renew. Sustain. Energy Rev. **69**, 535–550 (2017).
[27] A. Kitanovski, U. Plaznik, U. Tomc, and A. Poredoš, Int. J. Refrig. **57**, 288–298 (2015).
[28] J. Liang, K. Engelbrecht, K. K. Nielsen, K. Loewe, H. Vieyra, A. Barcza, and C. R. Bahl, Appl. Therm. Eng. **186**, 116519 (2021).
[29] K. Navickaitė, J. Liang, C. Bahl, S. Wieland, T. Buchenau, and K. Engelbrecht, Appl. Therm. Eng. **174**, 115297 (2020).
[30] Y. Zhu, J. Hur, S. Cheng, Q. Sun, W. Li, and S. Yao, Int. J. Heat Mass Transf. **176**, 121372 (2021).
[31] H. Hou, E. Simsek, T. Ma, N. S. Johnson, S. Qian, C. Cissé, D. Stasak, N. Al Hasan, L. Zhou, Y. Hwang, *et al.*, Science **366**, 1116–1121 (2019).
[32] N. Candau, C. Pradille, J.-L. Bouvard, and N. Billon, Polym. Test. **56**, 314–320 (2016).
[33] H. J. Qi and M. C. Boyce, Mech. Mater. **37**, 817–839 (2005).
[34] C. Prisacariu, *Polyurethane elastomers: from morphology to mechanical aspects* (Springer Science & Business Media, 2011).
[35] R. S. Rivlin and D. Saunders, Philos. Trans. R. Soc. **243**, 251–288 (1951).
[36] D. Haines and W. Wilson, J. Mech. Phys. Solids **27**, 345–360 (1979).
[37] Y. Wang, W. Luo, J. Huang, C. Peng, H. Wang, C. Yuan, G. Chen, B. Zeng, and L. Dai, Macromol. Theory Simul. **29**, 2000009 (2020).
[38] K. Upadhyay, G. Subhash, and D. Spearot, J. Mech. Phys. Solids **124**, 115–142 (2019).
[39] M. Pelliciari, S. Sirotti, and A. M. Tarantino, J. Mech. Phys. Solids **176**, 105308 (2023).
[40] M. F. Beatty and D. O. Stalnaker, J. Appl. Mech. **53**, 807–813 (1986).
[41] R. S. Rivlin, Trans. R. Soc. Lond. Ser. A Math. Phys. Sci. **241**, 379–397 (1948).
[42] R. W. Ogden, *Non-linear elastic deformations* (Courier Corporation, 1997).
[43] J. C. Simo and T. J. Hughes, *Computational inelasticity*, Vol. 7 (Springer Science & Business Media, 2006).
[44] R. Brighenti, Eng. Struct. **27**, 265–276 (2005).
[45] J. S. Bergström and M. Boyce, J. Mech. Phys. Solids **46**, 931–954 (1998).
[46] J. Tušek, K. Engelbrecht, D. Eriksen, S. Dall'Olio, J. Tušek, and N. Pryds, Nat. Energy **1**, 1–6 (2016).
[47] J. Tušek, K. Engelbrecht, R. Millán-Solsona, L. Manosa, E. Vives, L. P. Mikkelsen, and N. Pryds, Adv. Energy Mater. **5**, 1500361 (2015).
[48] K. Wang, J. T. B. Overvelde, K. Engelbrecht, R. Bjørk, and C. R. H. Bahl, "Data set for "volume compensation of large-deformation 3d-printed soft elastomeric elastocaloric regenerators"," data.dtu.dk (2023), 10.11583/DTU.23695065.